Petroleum Science 22 (2025) 1534–1547

Contents lists available at ScienceDirect

Petroleum Science

journal homepage: www.keaipublishing.com/en/journals/petroleum-science

Original Paper

Effective pure qP-wave equation and its numerical implementation in the time-space domain for 3D complicated anisotropic media

Shi-Gang Xu [a], Xing-Guo Huang [b,*], Li Han [b]

[a] Department of Geophysics, School of Geological Engineering and Geomatics, Chang'an University, Xi'an, 710064, Shaanxi, China
[b] College of Instrumentation and Electrical Engineering, Jilin University, Changchun, 130061, Jilin, China

ARTICLE INFO

Article history:
Received 17 July 2024
Received in revised form
29 October 2024
Accepted 16 February 2025
Available online 18 February 2025

Edited by Meng-Jiao Zhou and Teng Zhu

Keywords:
Anisotropic media
Wavefield extrapolation
Pure qP-wave equation
Optimization algorithm
Finite-difference method
Time-space domain

ABSTRACT

Seismic anisotropy has been extensively acknowledged as a crucial element that influences the wave propagation characteristic during wavefield simulation, inversion and imaging. Transversely isotropy (TI) and orthorhombic anisotropy (OA) are two typical categories of anisotropic media in exploration geophysics. In comparison of the elastic wave equations in both TI and OA media, pseudo-acoustic wave equations (PWEs) based on the acoustic assumption can markedly reduce computational cost and complexity. However, the presently available PWEs may experience SV-wave contamination and instability when anisotropic parameters cannot satisfy the approximated condition. Exploiting pure-mode wave equations can effectively resolve the above-mentioned issues and generate pure P-wave events without any artifacts. To further improve the computational accuracy and efficiency, we develop two novel pure qP-wave equations (PPEs) and illustrate the corresponding numerical solutions in the time-space domain for 3D tilted TI (TTI) and tilted OA (TOA) media. First, the rational polynomials are adopted to estimate the exact pure qP-wave dispersion relations, which contain complicated pseudo-differential operators with irrational forms. The polynomial coefficients are produced by applying a linear optimization algorithm to minimize the objective function difference between the expansion formula and the exact one. Then, the developed optimized PPEs are efficiently implemented using the finite-difference (FD) method in the time-space domain by introducing a scalar operator, which can help avoid the problem of spectral-based algorithms and other calculation burdens. Structures of the new equations are concise and corresponding implementation processes are straightforward. Phase velocity analyses indicate that our proposed optimized equations can lead to reliable approximation results. 3D synthetic examples demonstrate that our proposed FD-based PPEs can produce accurate and stable P-wave responses, and effectively describe the wavefield features in complicated TTI and TOA media.

1. Introduction

In exploration geophysics, abundant field data observations and laboratory measurements have validated that the seismic anisotropy widely exists in the subsurface medium (Thomsen, 1986; Tsvankin, 1997; Alkhalifah, 2000, 2003; Wang, 2002; Tsvankin and Grechka, 2011). Velocity anisotropy is a critical factor that affects the kinematics and dynamics behaviors of the seismic wave. Applying conventional isotropic wavefield extrapolation schemes to execute anisotropic inversion and imaging, these inaccurate propagation features may result in incorrectly timed and positioned wavefields, and further lead to misplaced profiles and low-resolution imaging of complex geological targets (Du et al., 2007; Fletcher et al., 2009; Fowler et al., 2010; Duveneck and Bakker, 2011; Zhang and Zhang, 2011; Zhang et al., 2011; Kazei and Alkhalifah, 2018). Therefore, developing seismic wave simulation, inversion and imaging based on the anisotropic assumption has a significant meaning for the development of high-accuracy geophysical techniques. Especially, seismic wavefield numerical modeling, which is characterized by adopting various numerical algorithms to solve different wave equations, is an engine for subsequent inversion and imaging.

Extensive research has demonstrated that transversely isotropy (TI) and orthorhombic anisotropy (OA) are two representative anisotropic models in sedimentary rocks (Tsvankin and Grechka, 2011; Guitton and Alkhalifah, 2017; Masmoudi and Alkhalifah, 2018). Anisotropic wave propagation can be adequately described by elastic wave equations with multiple independent parameters. However, anisotropic elastic counterparts are seldom applied in practice owing to their expensive computing cost and wavefield

* Corresponding author.
E-mail address: xingguo.huang19@gmail.com (X.-G. Huang).

https://doi.org/10.1016/j.petsci.2025.02.009

complexity. Therefore, exploiting wave equations only considering P-wave events for anisotropic media becomes an important research content. Up to now, plentiful anisotropic acoustic wave equations have been presented, which can be broadly divided into two categories: the coupled pseudo-acoustic wave equations (PWEs) (Du et al., 2007; Fletcher et al., 2009; Fowler et al., 2010; Duveneck and Bakker, 2011; Zhang and Zhang, 2011) and the decoupled pure qP-wave equations (PPEs) (Liu et al., 2009; Chu et al., 2011; Zhan et al., 2012; Xu and Zhou, 2014; Yan and Liu, 2016).

Starting from the dispersion relation of the anisotropic elastic wave equation and setting the SV-wave velocity along the symmetry axis to zero, Alkhalifah (2000, 2003) put forward coupled PWEs in vertical TI (VTI) and vertical OA (VOA) media. These PWEs are unphysical but they are convenient for seismic modeling, inversion and imaging purposes. Following Alkhalifah's works, a series of variations of PWEs have been developed (Du et al., 2007; Fletcher et al., 2009; Fowler et al., 2010; Duveneck and Bakker, 2011; Zhang and Zhang, 2011). However, these PWEs derived from the pseudo-acoustic assumption may encounter inevitable SV-wave contamination and propagation instability for undesirable anisotropic parameters (Fletcher et al., 2009). Accordingly, a lot of effort have been devoted to modify the commonly used PWEs, such as, introducing isotropic or elliptically anisotropic material surround the source (Alkhalifah, 2000), smoothing parameter models (Zhang and Zhang, 2008), setting nonzero shear wave velocity (Fletcher et al., 2009), and using filtering operations (Zhang et al., 2009). Unfortunately, these strategies cannot remove SV-wave artifacts fundamentally and stability disturbances for arbitrary anisotropic parameter conditions.

Alternatively, exploiting PPEs to generate anisotropic wavefields can thoroughly resolve the above-mentioned issues. Liu et al. (2009) derived isolated equations for P- and SV-waves through factoring the original P-SV dispersion relation and exhibit that the P-wave formula is completely free from SV-wave solution in VTI media. Because the decoupled pure-mode wave equations contain complex pseudo-differential operators, it is hard to solve them by common numerical algorithms. Therefore, to date, a lot of efforts were devoted to estimate complex pseudo-differential operators for the purpose of high computational accuracy, efficiency and flexibility (Liu et al., 2009; Chu et al., 2011; Zhan et al., 2012; Xu and Zhou, 2014; Yan and Liu, 2016; Fomel et al., 2013; Song and Alkhalifah, 2013; Zhang et al., 2019; Waheed et al., 2015; Li and Zhu, 2018; Sun and Alkhalifah, 2021). Particularly, Chu et al. (2011) applied a Taylor-series expansion (TE) method to approximate the complex pseudo-differential operator and calculate the tilted TI (TTI) PPE using the finite-difference (FD)-based iterative method. Zhan et al. (2012) computed a complex pseudo-differential operator in the wavenumber domain individually by a pseudo-spectral method and extend decoupled PPEs for modeling and reverse time migration (RTM) in acoustic TTI media. Song and Alkhalifah (2013) derived a pure qP-wave dispersion relation for tilted OA (TOA) media and then apply the low-rank approximation (LRA) method to compute it in the wavenumber domain. The LRA method generally has high computational accuracy, but the efficiency and flexibility are low due to the need for multiple Fourier transforms (Wu and Alkhalifah, 2014). Afterwards, Xu and Zhou (2014) developed a novel TTI PPE that can be conveniently solved by separating the complex pseudo-differential operator into two numerical operators: a differential equation and a scalar operator, which can be solved by the FD method in the time-space domain. The elliptical decomposition algorithm can produce exact phase information for the P-wave component at a lower cost than traditional methods. However, this efficient method sacrifices modeling accuracy for amplitude information. Thereafter, several modified approaches have been developed to compensate the amplitude error in acoustic TI and OA modeling (Waheed et al., 2015; Xu and Liu, 2018; Zhang et al., 2019). Recently, Li and Zhu (2018) adopted rational polynomials to expand the accurate pure P-wave dispersion relations for TI and OA media, and then generate expansion coefficients by using an optimization algorithm. The newly derived PPEs can be easily solved by combining the fast Poisson solver and the FD method, and produce acoustic wavefield with reliable amplitude and phase information. The extensions of the optimization expansion strategy have been successfully used for seismic modeling, inversion and imaging in TI and OA media (Zhang et al., 2019; Mu et al., 2020; Xu et al., 2023; Ren et al., 2024a, 2024b). Up to now, as for wavefield modeling in TI and OA media, many scholars pay more attention to create modified pure P-wave dispersion relations and PPEs with higher approximation accuracy and advanced numerical solutions with higher computational efficiency (Li and Stovas, 2021; Xu et al., 2020; Xu and Stovas, 2021; Liang et al., 2023; Bitencourt and Pestana, 2024; Mao et al., 2024).

In this paper, following previous works, we develop two PPEs and illustrate specific numerical solutions for wave propagation in complicated anisotropic media. First, a combination of a rational polynomial approximation and numerical optimization is used to estimate the exact pure P-wave dispersion relations, which involve complex pseudo-differential operators, and further construct two optimized PPEs for 3D TTI and TOA media. Then, the proposed equations can be decomposed into a differential formula and a scalar operator, and are efficiently calculated by using the unit vector approach and FD methods in the time-space domain. Finally, theoretical derivations, phase velocity analyses and modeling examples validate the advantages of our proposed methods.

2. Pure qP-wave equation in the time-space domain for TTI media

In this section, a recently proposed simplified PPE in 3D TTI media is first reviewed (Bitencourt and Pestana, 2024). Then, an optimized PPE with high approximation accuracy is developed based on previous studies. Last, the corresponding FD-based numerical solution with high computational efficiency in the time-space domain is presented.

2.1. A simplified pure qP-wave equation for 3D TTI media

The exact dispersion relation of the pure qP-wave in 3D TTI media can be expressed by

$$\omega^2=\frac{V_{\mathrm{pz}}^2}{2}\left(f\left(\widehat{k}_x,\widehat{k}_y,\widehat{k}_z\right)+\sqrt{f^2\left(\widehat{k}_x,\widehat{k}_y,\widehat{k}_z\right)-8(\varepsilon-\delta)\left(\widehat{k}_x^2+\widehat{k}_y^2\right)\widehat{k}_z^2}\right) \tag{1}$$

where, ω is the angular frequency, V_{pz} denotes the qP-wave velocity along the symmetry axis, ε and δ are the Thomsen's anisotropic parameters (Thomsen, 1986). $f(\widehat{k}_x,\widehat{k}_y,\widehat{k}_z) = (1+2\varepsilon)(\widehat{k}_x^2+\widehat{k}_y^2)+\widehat{k}_z^2$, where $\widehat{k}_x$, $\widehat{k}_y$ and $\widehat{k}_z$ are spatial wavenumber components along the symmetry axis evaluated in a rotated coordinate system. Specifically,

$$\begin{cases}\widehat{k}_x = k_x\cos\theta\cos\phi + k_y\cos\theta\sin\phi - k_z\sin\theta\\ \widehat{k}_y = -k_x\sin\phi + k_y\cos\phi\\ \widehat{k}_z = k_x\sin\theta\cos\phi + k_y\sin\theta\sin\phi + k_z\cos\theta\end{cases} \tag{2}$$

where θ denotes the dip angle of the symmetry axis measured from the vertical axis, and ϕ denotes the azimuth. k_x, k_y and k_z are spatial wavenumbers in the original coordinate system.

Eq. (1) can exactly depict qP-wave propagation characteristics in

3D TTI media, but it includes a square root term. It is difficult to solve such an equation numerically. To address this complex pseudo-differential operator, several polynomial expansion strategies were proposed to approximate the original dispersion relation, including, TE method (Chu et al., 2011; Zhan et al., 2012), spectral-based approximation (Yan and Liu, 2016; Fomel et al., 2013; Song and Alkhalifah, 2013), numerical optimization (Wu and Alkhalifah, 2014; Li and Zhu, 2018; Zhang et al., 2019), and so on. Among them, applying first-order TE to the square root term, Chu et al. (2011) derived an approximated dispersion relation for TTI pure qP-wave, which can greatly simplify calculation. Afterwards, Zhan et al. (2012) extended the related algorithm to TTI media and present a decoupled 3D PPE with a concise form. Based on Zhan et al. (2012)'s work, Bitencourt and Pestana (2024) further derived a simplified TTI PPE with higher computational efficiency as follows:

$$\frac{1}{V_{pz}^2}\frac{\partial^2 P(\boldsymbol{k},t)}{\partial t^2} = -\left\{\begin{array}{l} \tilde{a}_{11}k_x^2+\tilde{a}_{22}k_y^2+\tilde{a}_{33}k_z^2+\tilde{a}_{12}k_xk_y+\tilde{a}_{13}k_xk_z+\tilde{a}_{23}k_yk_z \\ +\tilde{a}_{1111}\frac{k_x^4}{k^2}+\tilde{a}_{2222}\frac{k_y^4}{k^2}+\tilde{a}_{3333}\frac{k_z^4}{k^2}+ \\ \frac{k_x^3}{k^2}(\tilde{a}_{1112}k_y+\tilde{a}_{1113}k_z)+\frac{k_y^3}{k^2}(\tilde{a}_{1222}k_x+\tilde{a}_{2223}k_z)+ \\ \frac{k_z^3}{k^2}(\tilde{a}_{1333}k_x+\tilde{a}_{2333}k_y) \end{array}\right\}P(\boldsymbol{k},t) \tag{3}$$

in which, $k^2 = k_x^2 + k_y^2 + k_z^2$, the wavenumber vector $\boldsymbol{k} = (k_x, k_y, k_z)$ describes the phase direction of the wave propagation. $P(\boldsymbol{k}, t)$ represents the pure qP-wave wavefield in the time-wavenumber domain. For convenience, the derivation process of Eq. (3) and polynomial coefficients $\tilde{a}_{11}$, $\tilde{a}_{22}$, $\tilde{a}_{33}$, $\tilde{a}_{12}$, $\tilde{a}_{13}$, $\tilde{a}_{23}$, $\tilde{a}_{1111}$, $\tilde{a}_{2222}$, $\tilde{a}_{3333}$, $\tilde{a}_{1112}$, $\tilde{a}_{1113}$, $\tilde{a}_{1222}$, $\tilde{a}_{2223}$, $\tilde{a}_{1333}$, $\tilde{a}_{2333}$ all are described in Appendix A.

At present, Eq. (3) is an advanced simplified PPE in 3D TTI media (Bitencourt and Pestana, 2024). Comparing Eq. (A1) and Eq. (3), the wavefield simulated effects are consistent. However, it can be found that the former occupies at least 16 (one forward and 15 inverse) FFTs for fractional terms to be computed, whereas the latter just needs 10 (one forward and 9 inverse) FFTs for one time loop. Therefore, this advanced simplified PPE for 3D TTI media is faster than the traditional one published in the geophysical literature (Bitencourt and Pestana, 2024).

2.2. An optimized pure qP-wave equation and its numerical implementation in the time-space domain for 3D TTI media

As validated in the related literature (Zhan et al., 2012; Bitencourt and Pestana, 2024), Eq. (A1) and Eq. (3) can accurately describe the pure qP-wave event in 3D TTI media. However, both Eq. (A1) and Eq. (3) are derived from the first-order TE strategy, which is a type of low-wavenumber/frequency estimation and can only keep high approximation accuracy for relatively low wavenumber/frequency ranges (Li and Zhu, 2018; Zhang et al., 2019; Mu et al., 2020; Xu et al., 2023). To further improve the approximation accuracy, we develop an optimized PPE and illustrate its numerical implementation scheme in the time-space domain for 3D TTI media.

Similar to Eq. (3), we first apply an algebraic expression to expand the original exact dispersion relation (Eq. (1)) in the wavenumber domain as follows:

$$G(\boldsymbol{b},\boldsymbol{k}) \approx b_1k_x^2+b_2k_y^2+b_3k_z^2+b_4k_xk_y+b_5k_xk_z+b_6k_yk_z+b_7\frac{k_x^4}{k'^2} +b_8\frac{k_y^4}{k'^2}+b_9\frac{k_z^4}{k'^2}+b_{10}\frac{k_x^3k_y}{k'^2}+b_{11}\frac{k_x^3k_z}{k'^2}+b_{12}\frac{k_xk_y^3}{k'^2}+b_{13}\frac{k_y^3k_z}{k'^2} +b_{14}\frac{k_xk_z^3}{k'^2}+b_{15}\frac{k_yk_z^3}{k'^2} \tag{4}$$

where, $\boldsymbol{k}$ is a vector of k_x, k_y and k_z, $\boldsymbol{b}$ is a vector of $b_1 - b_{15}$, and $k'^2 = (1+2\varepsilon)(k_x^2+k_y^2)+k_z^2$. Compared to the original dispersion relation (Eq. (1)), the polynomial coefficients $b_1 - b_{15}$ and orthogonal spatial wavenumbers k_x, k_y, k_z in the expansion formula (Eq. (4)) are decoupled, thus the form is straightforward.

By minimizing the difference between Eq. (1) and Eq. (4) within a limited wavenumber/frequency region, we are able to yield globally optimal coefficients $b_1 - b_{15}$. On the basis of Eq. (1) and Eq. (4), we construct an objective function as follows:

$$J(\boldsymbol{b}) = \iiint [A(\hat{\boldsymbol{k}}) - G(\boldsymbol{b},\boldsymbol{k})]^2 \mathrm{d}k_x\mathrm{d}k_y\mathrm{d}k_z \tag{5}$$

where, $\hat{\boldsymbol{k}}$ is a vector of $\hat{k}_x$, $\hat{k}_y$, $\hat{k}_z$, and

$$A(\hat{\boldsymbol{k}}) = \left(f(\hat{k}_x,\hat{k}_y,\hat{k}_z)+\sqrt{f^2(\hat{k}_x,\hat{k}_y,\hat{k}_z)-8(\varepsilon-\delta)\left(\hat{k}_x^2+\hat{k}_y^2\right)\hat{k}_z^2}\right)\Big/2 \tag{6}$$

Eq. (5) is a standard linear regression problem and can be expediently calculated by adopting some linear optimization algorithms. The corresponding coefficients are functions of spatial locations because they depend on the anisotropic parameters and angle parameters. Once an anisotropic model is provided, one can solve the above optimization system for each spatial node and generate optimized coefficients $b_1 - b_{15}$.

By using the novel approximation formula (Eq. (4)), the proposed optimized pure qP-wave dispersion relation for 3D TTI media is written as

$$\omega^2 \approx V_{pz}^2\left(\begin{array}{l} b_1k_x^2+b_2k_y^2+b_3k_z^2+b_4k_xk_y+b_5k_xk_z+b_6k_yk_z+b_7\frac{k_x^4}{k'^2}+b_8\frac{k_y^4}{k'^2}+ \\ b_9\frac{k_z^4}{k'^2}+b_{10}\frac{k_x^3k_y}{k'^2}+b_{11}\frac{k_x^3k_z}{k'^2}+b_{12}\frac{k_y^3k_x}{k'^2}+b_{13}\frac{k_y^3k_z}{k'^2}+b_{14}\frac{k_z^3k_x}{k'^2}+b_{15}\frac{k_z^3k_y}{k'^2} \end{array}\right) \tag{7}$$

Previous experiences have shown that it is hard to solve PPEs (Eqs. (A1), (3) and (7)) by using some common numerical algorithms owing to the existence of the fractional terms (Chu et al., 2011; Zhan et al., 2012; Yan and Liu, 2016; Li and Zhu, 2018). Thus, to improve the computational efficiency and flexibility on the premise of ensuring accuracy, we next provide a practical implementation solution for the proposed optimized PPE in the time-space domain.

By referring to the definition of the scalar operator S for acoustic TTI wavefield simulation (Xu and Zhou, 2014; Liang et al., 2023), we introduce a unified scalar operator S_α^k in the wavenumber domain as follows:

$$S_\alpha^k = \frac{k_\alpha^2}{(1+2\varepsilon)\left(k_x^2+k_y^2\right)+k_z^2}, \alpha \in \{x,y,z\} \tag{8}$$

Then, taking the scalar operator S_α^k into the proposed dispersion relation (Eq. (7)), it can be arranged as

$$\omega^2 \approx V_{\mathrm{pz}}^2 \begin{pmatrix} \left(b_1+b_7S_x^k\right)k_x^2+\left(b_2+b_8S_y^k\right)k_y^2+\left(b_3+b_9S_z^k\right)k_z^2+ \\ \left(b_4+b_{10}S_x^k+b_{12}S_y^k\right)k_xk_y+\left(b_5+b_{11}S_x^k+b_{14}S_z^k\right)k_xk_z \\ +\left(b_6+b_{13}S_y^k+b_{15}S_z^k\right)k_yk_z \end{pmatrix} \tag{9}$$

Applying FFT to Eq. (9), we obtain an optimized PPE in the mixed space-wavenumber domain for 3D TTI media as follows:

$$\frac{\partial^2 P(\boldsymbol{x},\boldsymbol{k},t)}{\partial t^2} = V_{\mathrm{pz}}^2 \begin{pmatrix} \left(b_1+b_7S_x^k\right)D_{xx}+\left(b_2+b_8S_y^k\right)D_{yy}+\left(b_3+b_9S_z^k\right)D_{zz} \\ +\left(b_4+b_{10}S_x^k+b_{12}S_y^k\right)D_xD_y \\ +\left(b_5+b_{11}S_x^k+b_{14}S_z^k\right)D_xD_z \\ +\left(b_6+b_{13}S_y^k+b_{15}S_z^k\right)D_yD_z \end{pmatrix} P(\boldsymbol{x},\boldsymbol{k},t) \tag{10}$$

where $D_{\alpha\alpha}=\frac{\partial^2}{\partial\alpha^2}$ and $D_\alpha=\frac{\partial}{\partial\alpha}$ represent the second- and first-order spatial partial differential operators, respectively.

Once we obtain the value of the scalar operator S_α^k in the above equation, the optimized PPE can be conveniently solved by the commonly used FD methods. Thus, we introduce an effective solution to the scalar operator S_α^k.

Then, the unit vector of the phase direction $\boldsymbol{n}$ can be calculated by (Xu and Zhou, 2014; Liang et al., 2023)

$$\boldsymbol{n} = (n_x, n_y, n_z) = \left(\frac{k_x}{k}, \frac{k_y}{k}, \frac{k_z}{k}\right) = \frac{\boldsymbol{k}}{|\boldsymbol{k}|} \tag{11}$$

Substituting the propagation direction $\boldsymbol{n}$ into Eq. (8), the operator S_α^k can be represented by the operator S_α^n as follows:

$$S_\alpha^n = \frac{n_\alpha^2}{(1+2\varepsilon)\left(n_x^2+n_y^2\right)+n_z^2} \tag{12}$$

Xu and Zhou (2014) developed the asymptotic form for Eq. (11) in the space domain and the phase direction vector $\boldsymbol{n}$ can be specifically computed by using the local phase direction (Xu and Zhou, 2014; Liang et al., 2023):

$$n_\alpha = \frac{D_\alpha P}{\sqrt{(D_xP)^2+(D_yP)^2+(D_zP)^2}} \alpha \in \{x,y,z\} \tag{13}$$

Based on the above equation, the operators S_α^n are rewritten in the following forms:

$$\begin{aligned} S_x^n &= \frac{1}{(1+2\varepsilon)\left(1+\left(\frac{D_yP}{D_xP}\right)^2\right)+\left(\frac{D_zP}{D_xP}\right)^2}, \\ S_y^n &= \frac{1}{(1+2\varepsilon)\left(\left(\frac{D_xP}{D_yP}\right)^2+1\right)+\left(\frac{D_zP}{D_yP}\right)^2}, \\ S_z^n &= \frac{1}{(1+2\varepsilon)\left(\left(\frac{D_xP}{D_zP}\right)^2+\left(\frac{D_yP}{D_zP}\right)^2\right)+1}. \end{aligned} \tag{14}$$

Then, substituting Eq. (14) into Eq. (10) and replacing the operators S_α^k with the operators S_α^n, the proposed PPE in the time-space domain becomes

$$\frac{\partial^2 P(\boldsymbol{x},t)}{\partial t^2} = V_{\mathrm{pz}}^2 \begin{pmatrix} (b_1+b_7S_x^n)D_{xx}+\left(b_2+b_8S_y^n\right)D_{yy}+(b_3+b_9S_z^n)D_{zz}+ \\ \left(b_4+b_{10}S_x^n+b_{12}S_y^n\right)D_xD_y+(b_5+b_{11}S_x^n+b_{14}S_z^n)D_xD_z \\ +\left(b_6+b_{13}S_y^n+b_{15}S_z^n\right)D_yD_z \end{pmatrix} P(\boldsymbol{x},t) \tag{15}$$

It is evident that the righthand side of Eq. (15) is all spatial terms, and there are no extra terms of the wavenumber, thus it is convenient to execute wavefield simulation.

In the time-space domain, we apply regular-grid FD method to solve the proposed PPE (Eq. (15)) and carry out the wavefield extrapolation in 3D TTI media. The 3D FD solvers in the time and space domains are respectively defined as

$$\begin{cases} \dfrac{\partial^2 P}{\partial t^2} = \dfrac{1}{\Delta t^2}\left(P_{i,j,l}^{o+1} - 2P_{i,j,l}^{o} + P_{i,j,l}^{o-1}\right), \\ D_{xx}P = \dfrac{\partial^2 P}{\partial x^2} = \dfrac{1}{\Delta x^2}\left[c_0'' P_{i,j,l}^{o} + \sum_{m=1}^{M} c_m''\left(P_{i+m,j,l}^{o} + P_{i-m,j,l}^{o}\right)\right], \\ D_{yy}P = \dfrac{\partial^2 P}{\partial y^2} = \dfrac{1}{\Delta y^2}\left[c_0'' P_{i,j,l}^{o} + \sum_{m=1}^{M} c_m''\left(P_{i,j+m,l}^{o} + P_{i,j-m,l}^{o}\right)\right], \\ D_{zz}P = \dfrac{\partial^2 P}{\partial z^2} = \dfrac{1}{\Delta z^2}\left[c_0'' P_{i,j,l}^{o} + \sum_{m=1}^{M} c_m''\left(P_{i,j,l+m}^{o} + P_{i,j,l-m}^{o}\right)\right], \\ D_{x}P = \dfrac{\partial P}{\partial x} = \dfrac{1}{\Delta x}\sum_{m=1}^{M} c_m'\left(P_{i+m,j,l}^{o} - P_{i-m,j,l}^{o}\right), \\ D_{y}P = \dfrac{\partial P}{\partial y} = \dfrac{1}{\Delta y}\sum_{m=1}^{M} c_m'\left(P_{i,j+m,l}^{o} - P_{i,j-m,l}^{o}\right), \\ D_{z}P = \dfrac{\partial P}{\partial z} = \dfrac{1}{\Delta z}\sum_{m=1}^{M} c_m'\left(P_{i,j,l+m}^{o} - P_{i,j,l-m}^{o}\right), \end{cases} \tag{16}$$

where Δt is the temporal sampling interval, Δx, Δy and Δz are spatial grid spacings along different directions. M denotes a half of the FD operator length, c_m' and c_m'' are optimized high-order FD coefficients for the first- and second-order spatial derivatives, respectively (Liu, 2013).

Substituting the discretization terms of Eq. (16) into Eq. (15), we obtain an effective FD-based wavefield extrapolation scheme for 3D TTI media as follows:

$$P_{i,j,l}^{o+1} = 2P_{i,j,l}^{o} + P_{i,j,l}^{o-1} + \Delta t^2 V_{pz}^2 \begin{pmatrix} \left(b_1 + b_7 S_x^d\right)D_{xx} + \left(b_2 + b_8 S_y^d\right)D_{yy} + \left(b_3 + b_9 S_z^d\right)D_{zz} + \\ \left(b_4 + b_{10}S_x^d + b_{12}S_y^d\right)D_xD_y + \left(b_5 + b_{11}S_x^d + b_{14}S_z^d\right)D_xD_z \\ + \left(b_6 + b_{13}S_y^d + b_{15}S_z^d\right)D_yD_z \end{pmatrix} P_{i,j,l}^{o} \tag{17}$$

where the operators S_x^d, S_y^d and S_z^d are difference discretization forms of the operators S_x^n, S_y^n and S_z^n.

In conclusion, adopting an optimization algorithm to solve the objective function (Eq. (5)), we compute polynomial coefficients $b_1 - b_{15}$. Then, the effective wavefield extrapolation in 3D TTI media can be accomplished based on Eq. (17).

3. Extending the pure qP-wave equation to 3D TOA media

In the previous section, we develop an advanced PPE and illustrate the corresponding FD-based numerical solution in the time-space domain for 3D TTI media. Here, we extend the related algorithms to the more complicated TOA media.

Through calculating the eigenvalues of PWEs in 3D TOA media, we can derive an exact dispersion relation in the frequency-wavenumber domain as follows (Xu and Zhou, 2014):

$$\omega^2 = \frac{V_{pz}^2}{3}\left(-a - \sqrt[3]{(d+g)/2} - \sqrt[3]{(d-g)/2}\right) \tag{18}$$

in which

$$\begin{cases} a = -\left((1+2\varepsilon_2)\hat{k}_x^2 + (1+2\varepsilon_1)\hat{k}_y^2 + \hat{k}_z^2\right), \\ b = \begin{pmatrix} 2(\varepsilon_2-\delta_2)\hat{k}_x^2\hat{k}_z^2 + 2(\varepsilon_1-\delta_1)\hat{k}_y^2\hat{k}_z^2 + \\ ((1+2\varepsilon_2)(1+2\varepsilon_1) - (1+2\varepsilon_2)(1+2\delta_3))\hat{k}_x^2\hat{k}_y^2 \end{pmatrix}, \\ c = \begin{pmatrix} -(1+2\varepsilon_2)(1+2(\varepsilon_1-\delta_1)) + (1+2\varepsilon_2)^2(1+2\delta_3) \\ -2(1+2\varepsilon_2)\sqrt{(1+2\delta_1)(1+2\delta_2)(1+2\delta_3)} \\ +(1+2\varepsilon_1)(1+2\delta_2) \end{pmatrix}\hat{k}_x^2\hat{k}_y^2\hat{k}_z^2, \\ d = 2a^3 - 9ab + 27c, \\ g = \sqrt{d^2 - 4\left(a^2-3b\right)^3}, \end{cases} \tag{19}$$

where, ε_1 and ε_2 represent the VTI parameter ε in the *yoz* and *xoz* planes, δ_1, δ_2 and δ_3 denote the VTI parameter δ in the *yoz*, *xoz* and *xoy* planes, respectively (Tsvankin, 1997). Eq. (18) is degenerated into 3D TTI media by setting $\varepsilon_1 = \varepsilon_2 = \varepsilon$, $\delta_1 = \delta_2 = \delta$ and $\delta_3 = 0$.

Previous works have shown that Eq. (18) can accurately describe the pure qP-wave event in 3D TOA media (Xu and Zhou, 2014; Xu and Liu, 2018; Zhang et al., 2019). Evidently, it is difficult to solve the exact pure qP-wave dispersion relation by using common numerical algorithms. Similar to 3D TTI media, we adopt the following polynomial expression to expand the term $-a - \sqrt[3]{(d+g)/2} - \sqrt[3]{(d-g)/2}$ in Eq. (18):

$$S(\boldsymbol{d},\boldsymbol{k}) \approx d_1k_x^2+d_2k_y^2+d_3k_z^2+d_4k_xk_y+d_5k_xk_z+d_6k_yk_z+d_7\frac{k_x^4}{k^2}+d_8\frac{k_y^4}{k^2}+d_9\frac{k_z^4}{k^2}+d_{10}\frac{k_x^3k_y}{k^2}+d_{11}\frac{k_x^3k_z}{k^2}+d_{12}\frac{k_y^3k_x}{k^2}+d_{13}\frac{k_y^3k_z}{k^2}+d_{14}\frac{k_z^3k_x}{k^2}+d_{15}\frac{k_z^3k_y}{k^2} \tag{20}$$

where $\boldsymbol{d}$ is a vector of $d_1 - d_{15}$. Analogously, the coefficients $d_1 - d_{15}$ can be generated by solving a linear objective system based on the optimization strategy, as described in Eq. (5).

Substituting Eq. (20) into Eq. (18), the high-accuracy approximated dispersion relation for 3D TOA media is denoted by

$$\omega^2 \approx V_{\mathrm{pz}}^2\left(\begin{array}{l} d_1k_x^2+d_2k_y^2+d_3k_z^2+d_4k_xk_y+d_5k_xk_z+d_6k_yk_z+ \\ d_7\frac{k_x^4}{k^2}+d_8\frac{k_y^4}{k^2}+d_9\frac{k_z^4}{k^2}+d_{10}\frac{k_x^3k_y}{k^2}+d_{11}\frac{k_x^3k_z}{k^2}+ \\ d_{12}\frac{k_y^3k_x}{k^2}+d_{13}\frac{k_y^3k_z}{k^2}+d_{14}\frac{k_z^3k_x}{k^2}+d_{15}\frac{k_z^3k_y}{k^2} \end{array}\right) \tag{21}$$

Based on the aforementioned scalar operators S_α^k $(\alpha\in\{x,y,z\})$, the proposed dispersion relation (Eq. (21)) is rearranged as

$$\omega^2 \approx V_{\mathrm{pz}}^2\left(\begin{array}{l} \left(d_1+d_7S_x^k\right)k_x^2+\left(d_2+d_8S_y^k\right)k_y^2+\left(d_3+d_9S_z^k\right)k_z^2+ \\ \left(d_4+d_{10}S_x^k+d_{12}S_y^k\right)k_xk_y+\left(d_5+d_{11}S_x^k+d_{14}S_z^k\right)k_xk_z \\ +\left(d_6+d_{13}S_y^k+d_{15}S_z^k\right)k_yk_z \end{array}\right) \tag{22}$$

Transforming it back to the time-space domain and combining the scalar operators S_α^n $(\alpha\in\{x,y,z\})$, we obtain a novel PPE for 3D TOA media as

$$\frac{\partial^2 P(\boldsymbol{x},t)}{\partial t^2}=V_{\mathrm{pz}}^2\left(\begin{array}{l} (d_1+d_7S_x^n)D_{xx}+\left(d_2+d_8S_y^n\right)D_{yy}+(d_3+d_9S_z^n)D_{zz} \\ +\left(d_4+d_{10}S_x^n+d_{12}S_y^n\right)D_xD_y \\ +(d_5+d_{11}S_x^n+d_{14}S_z^n)D_xD_z \\ +\left(d_6+d_{13}S_y^n+d_{15}S_z^n\right)D_yD_z \end{array}\right)P(\mathbf{x},t) \tag{23}$$

Likewise, this equation can be easily computed by the commonly used FD method. The corresponding high-accuracy wavefield extrapolation scheme can be written as

Table 1
Polynomial coefficients of optimized pure qP-wave dispersion relations in homogeneous TTI and TOA media.

b	Homogeneous TTI media		d	Homogeneous TOA media	
	Model I	Model II		Model I	Model II
b_1	1.379302e+0	8.265387e−1	d_1	1.352738e+0	6.932912e−1
b_2	1.379302e+0	8.265387e−1	d_2	1.352738e+0	6.932912e−1
b_3	1.294412e+0	9.237412e−1	d_3	6.219801e−1	2.010786e+0
b_4	−4.893111e−1	−5.186113e−1	d_4	−4.926537e−1	−5.059455e−1
b_5	2.384338e−1	3.902666e−2	d_5	1.964725e−1	5.072065e−2
b_6	2.384338e−1	3.902666e−2	d_6	1.964725e−1	5.072065e−2
b_7	−2.803182e−1	6.685650e−2	d_7	−1.485011e−1	3.483390e−1
b_8	−2.803182e−1	6.685650e−2	d_8	−1.485011e−1	3.483390e−1
b_9	−3.586984e−3	1.084212e−1	d_9	3.786083e−1	−7.467122e−1
b_{10}	−9.792786e−2	5.734586e−1	d_{10}	−5.954408e−2	8.893035e−1
b_{11}	−9.596415e−1	2.666647e−1	d_{11}	−2.121752e−1	−4.697092e−1
b_{12}	−9.792786e−2	5.734586e−1	d_{12}	−5.954408e−2	8.893035e−1
b_{13}	−9.596415e−1	2.666647e−1	d_{13}	−2.121752e−1	−4.697092e−1
b_{14}	−7.513516e−1	1.174174e−1	d_{14}	−1.017209e−1	−3.778949e−1
b_{15}	−7.513516e−1	1.174174e−1	d_{15}	−1.017209e−1	−3.778949e−1

$$P_{i,j,l}^{o+1}=2P_{i,j,l}^{o}+P_{i,j,l}^{o-1}+\Delta t^2V_{\mathrm{pz}}^2\left(\begin{array}{l} \left(d_1+d_7S_x^d\right)D_{xx}+\left(d_2+d_8S_y^d\right)D_{yy}+ \\ \left(d_3+d_9S_z^d\right)D_{zz}+\left(d_4+d_{10}S_x^d+d_{12}S_y^d\right)D_xD_y \\ +\left(d_5+d_{11}S_x^d+d_{14}S_z^d\right)D_xD_z \\ +\left(d_6+d_{13}S_y^d+d_{15}S_z^d\right)D_yD_z \end{array}\right)P_{i,j,l}^{o} \tag{24}$$

where the operators S_x^d, S_y^d and S_z^d are difference discretization forms of the operators S_x^n, S_y^n and S_z^n.

Similarly, optimized coefficients $d_1 - d_{15}$ can be computed using linear optimization strategy. Adopting Eq. (24) can provide pure qP-wave propagation in 3D TOA media.

4. Phase velocity accuracy analysis

To verify the numerical accuracy of different pure qP-wave dispersion relations, we compute phase velocities in two homogeneous TTI models with Eqs. (3) and (7), and compare them with the accurate phase velocities, which are generated by Eq. (1).

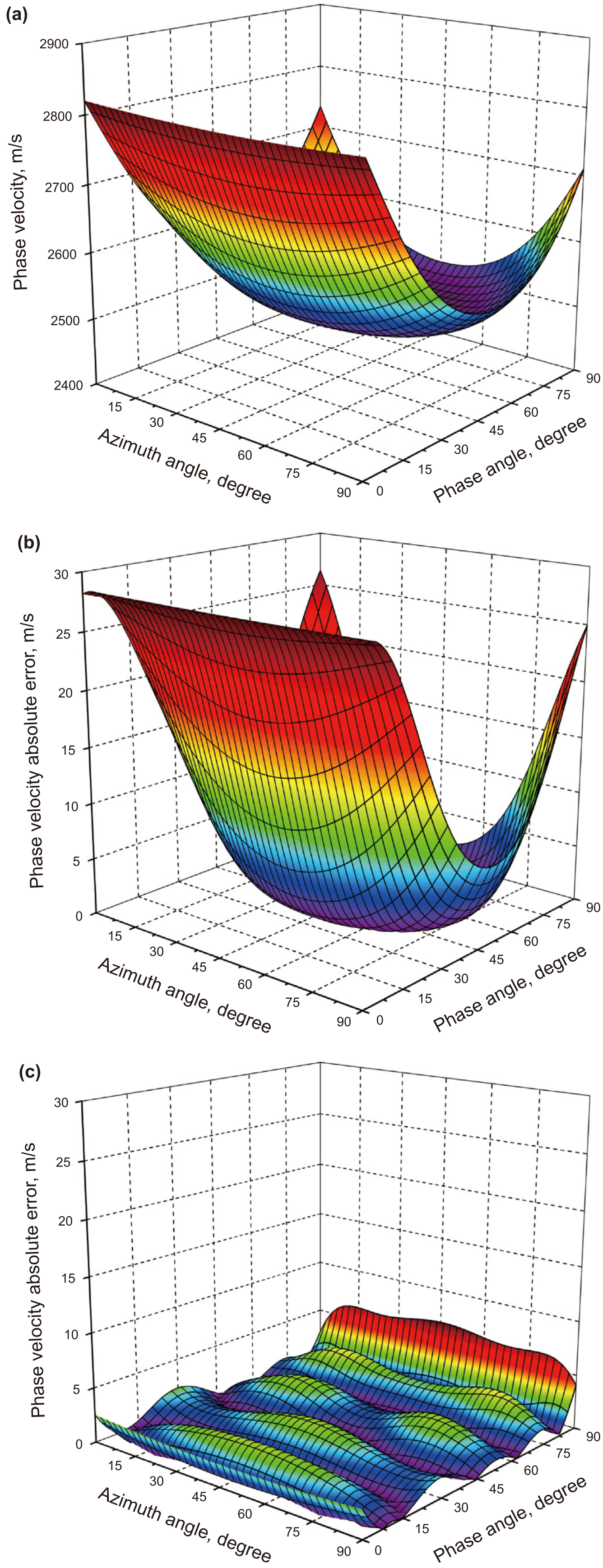

Fig. 1. Phase velocity and absolute error analysis in a 3D homogeneous TTI medium with $\varepsilon = 0.25$, $\delta = -0.05$, $\theta = 60^{\circ}$ and $\phi = 45^{\circ}$. **(a)** is the exact phase velocity surface of Eq. (1), **(b)** is the absolute error surface of the simplified dispersion relation (Eq. (3)), and **(c)** is the absolute error surface of the proposed optimized dispersion relation (Eq. (7)).

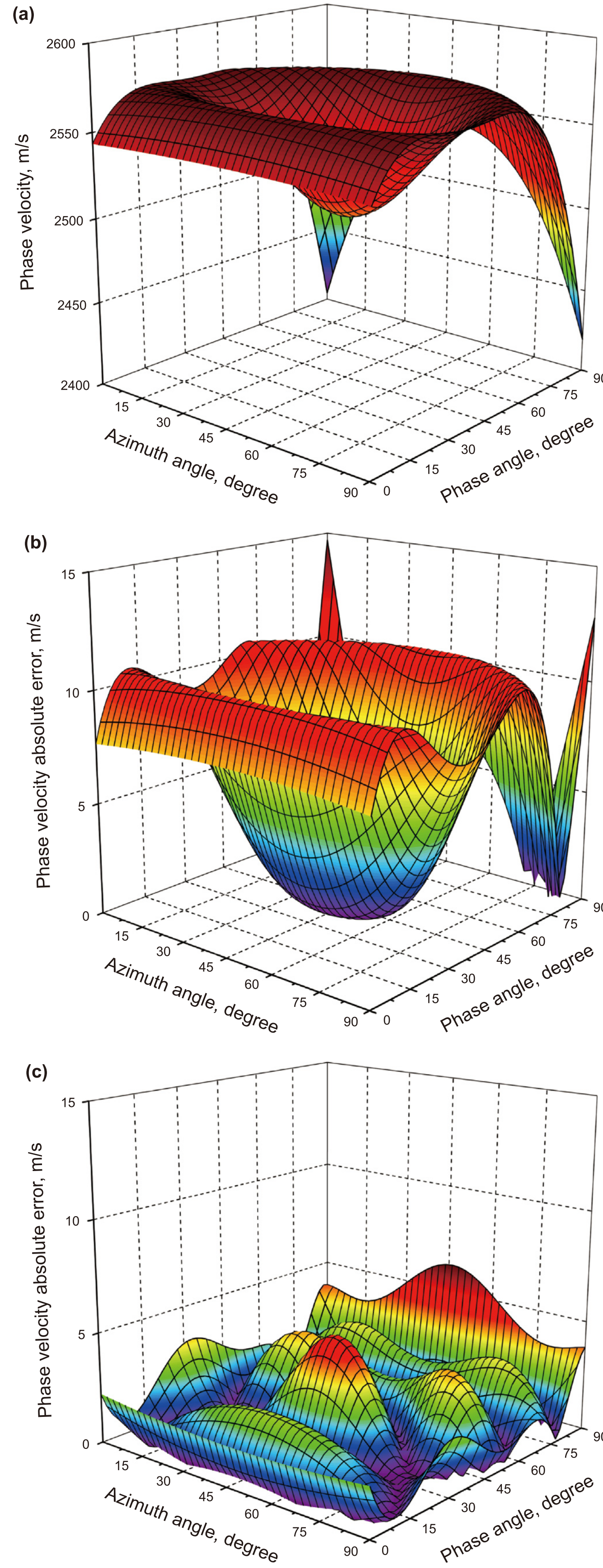

Fig. 2. Phase velocity and absolute error analysis in a 3D homogeneous TTI medium with $\varepsilon = -0.15$, $\delta = 0.22$, $\theta = 45^{\circ}$ and $\phi = 45^{\circ}$. **(a)** is the exact phase velocity surface of Eq. (1), **(b)** is the absolute error surface of the simplified dispersion relation (Eq. (3)), and **(c)** is the absolute error surface of the proposed optimized dispersion relation (Eq. (7)).

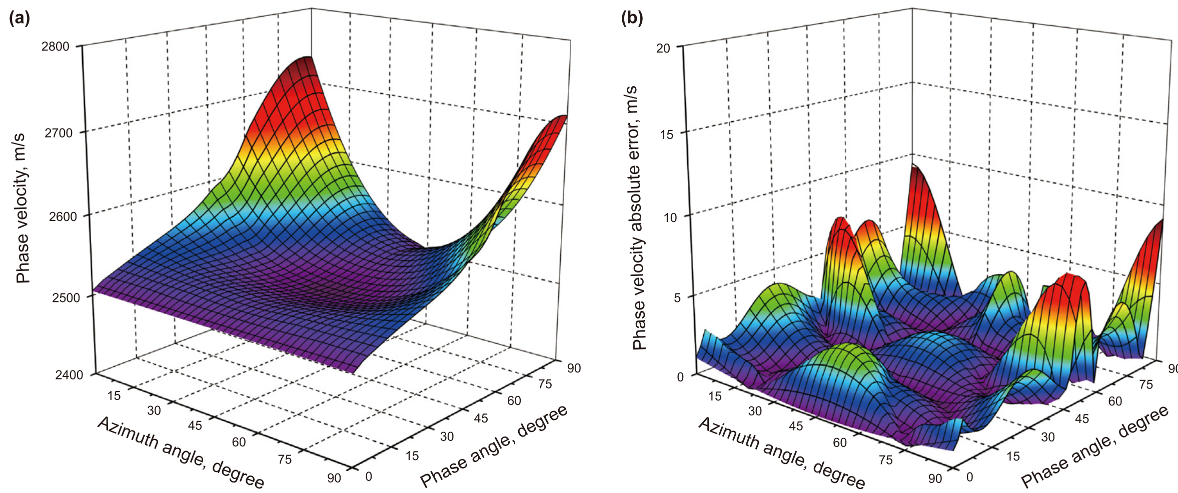

Fig. 3. Phase velocity and absolute error analysis in a 3D homogeneous TOA medium with $\varepsilon_1 = 0.28$, $\varepsilon_2 = -0.05$, $\delta_1 = \delta_2 = \delta_3 = 0.06$ and $\theta = \phi = 45^\circ$. **(a)** Is the exact phase velocity surface of Eq. (18), **(b)** is the absolute error surface of the proposed optimized dispersion relation (Eq. (21)).

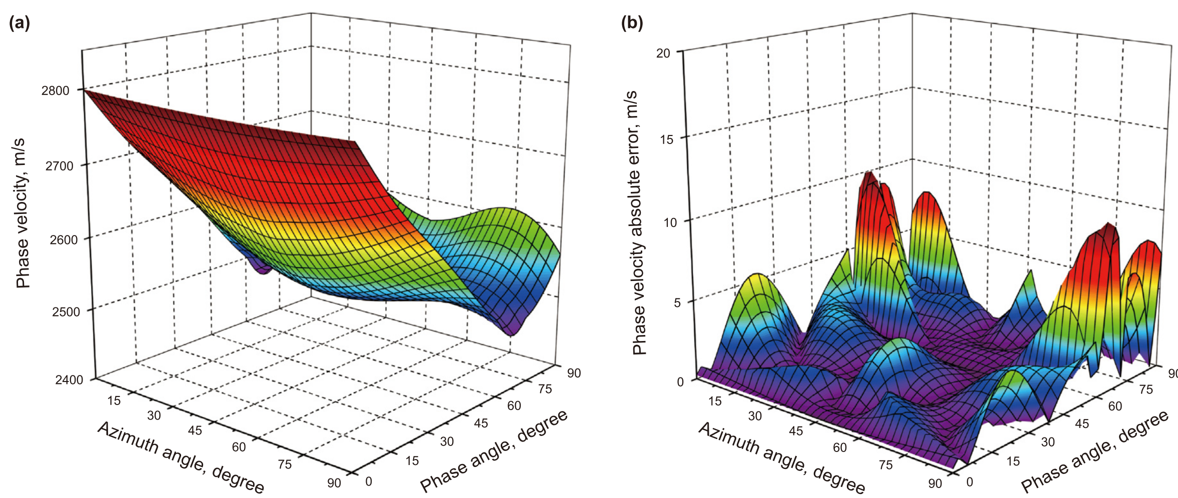

Fig. 4. Phase velocity and absolute error analysis in a 3D homogeneous TOA medium with $\varepsilon_1 = -0.15$, $\varepsilon_2 = 0.20$, $\delta_1 = \delta_2 = \delta_3 = 0.08$, $\theta = 60^\circ$ and $\phi = 45^\circ$. **(a)** is the exact phase velocity surface of Eq. (18), and **(b)** is the absolute error surface of the proposed optimized dispersion relation (Eq. (21)).

Table 1 shows the corresponding optimized polynomial coefficients in our proposed scheme. Figs. 1 and 2 depict several exact phase velocity surfaces and absolute error surfaces for two TTI models. The vertical P-wave propagation velocity is 2500 m/s. The related anisotropic parameters and angle parameters are all described in the figure caption. From these figures, we can conclude that, the phase velocity errors of the present advanced pure qP-wave dispersion relation (Eq. (3)) are relatively large because the calculated results are far from the zero-value plane. By contrast, our proposed optimized equation (Eq. (7)) can uniformly distribute the phase velocity errors, and generate high-accuracy simulated results.

To further examine the numerical accuracy of our optimized equation (Eq. (21)) in 3D TOA media, two TOA models are designed to compute phase velocities and their absolute errors, which are displayed in Figs. 3 and 4. The optimized polynomial coefficients are provided in Table 1. The vertical P-wave velocity is 2500 m/s, and other parameters are illustrated in the figure caption. From these figures, we can see that the novel optimized equation can produce acceptable numerical accuracy compared with the reference surface under different parameter conditions, even for strong anisotropic media. The phase velocity accuracy analyses demonstrate that our developed optimized PPEs can produce reliable approximation results for the following wavefield extrapolation in 3D TTI and TOA media.

5. Numerical examples

In this section, several synthetic simulation examples are applied to validate the efficacy of the proposed PPEs. For comparison, modeling results of PWEs (Du et al., 2007; Zhang and Zhang, 2011) are also presented. It should be noticed that both conventional PWEs and the proposed PPEs are discretized by temporal second-order and spatial high-order FD operators.

5.1. 3D homogeneous anisotropic media

In the first example, we examine our developed algorithm using two homogeneous anisotropic models. The model size is 2000 m × 2000 m × 2000 m, and the cubic grid interval is 10 m. A Ricker wavelet, with a peak frequency of 30 Hz, is located at the middle of the model to produce the vibration. The vertical P-wave

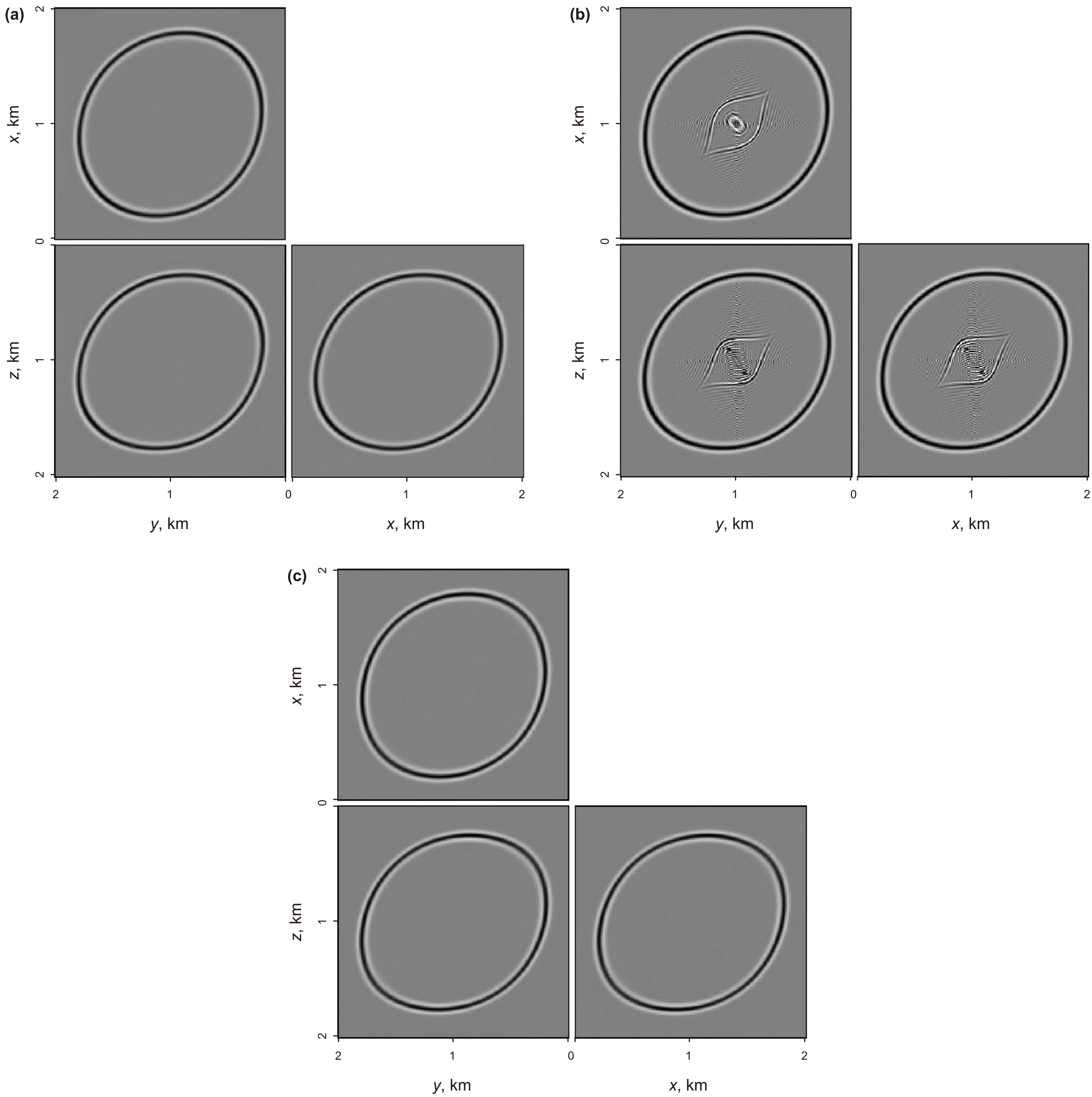

Fig. 5. Wavefield snapshots in 3D TTI media of **(a)** the reference solution, **(b)** the conventional PWE and **(c)** the proposed PPE, respectively. The related parameters are $\varepsilon = 0.26$, $\delta = 0.08$ and $\theta = \phi = 45^\circ$.

propagation velocity is 2600 m/s, and other anisotropic parameters and angle parameters are listed in the figure caption. In particular, we also provide several reference solutions, which are produced by adopting the pseudospectral method to compute the exact pure qP-wave equations (Eqs. (1) and (18)) (Chu et al., 2011; Zhan et al., 2012), are illustrated in Appendix B. Figs. 5 and 6 display several time snapshots of wave propagation in 3D TTI and TOA media, respectively. Comparing the modeling results of the exact solutions, conventional equations and our proposed equations, we can conclude that: (1) Inevitably, the wavefield slices generated by the conventional PWEs contain strong SV-waves near the wave source, which affect the external P-wave characteristics. In particular, the wavefield of PWE in TOA media becomes unstable owing to undesirable anisotropic parameters and angle parameters, thus we don't show the calculated result. (2) By contrast, snapshots of our FD-based optimized PPEs are completely free of SV-waves while preserving P-wave events very well. Besides, the proposed schemes have favorable stability for different parameter combinations.

5.2. 3D complicated anisotropic media

Because there are no “known to us” available heterogeneous

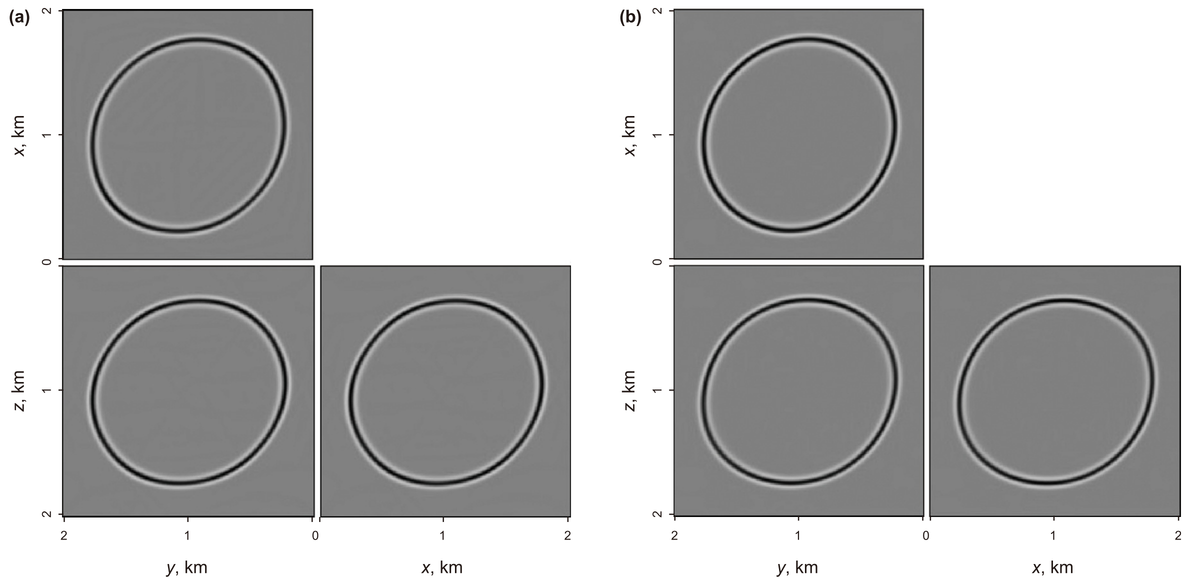

Fig. 6. Wavefield snapshots in 3D TOA media of **(a)** the reference solution and **(b)** the proposed PPE, respectively. The related parameters are $\varepsilon_1 = 0.20$, $\varepsilon_2 = 0.15$, $\delta_1 = \delta_2 = \delta_3 = 0.06$, $\theta = 45^\circ$ and $\phi = 45^\circ$.

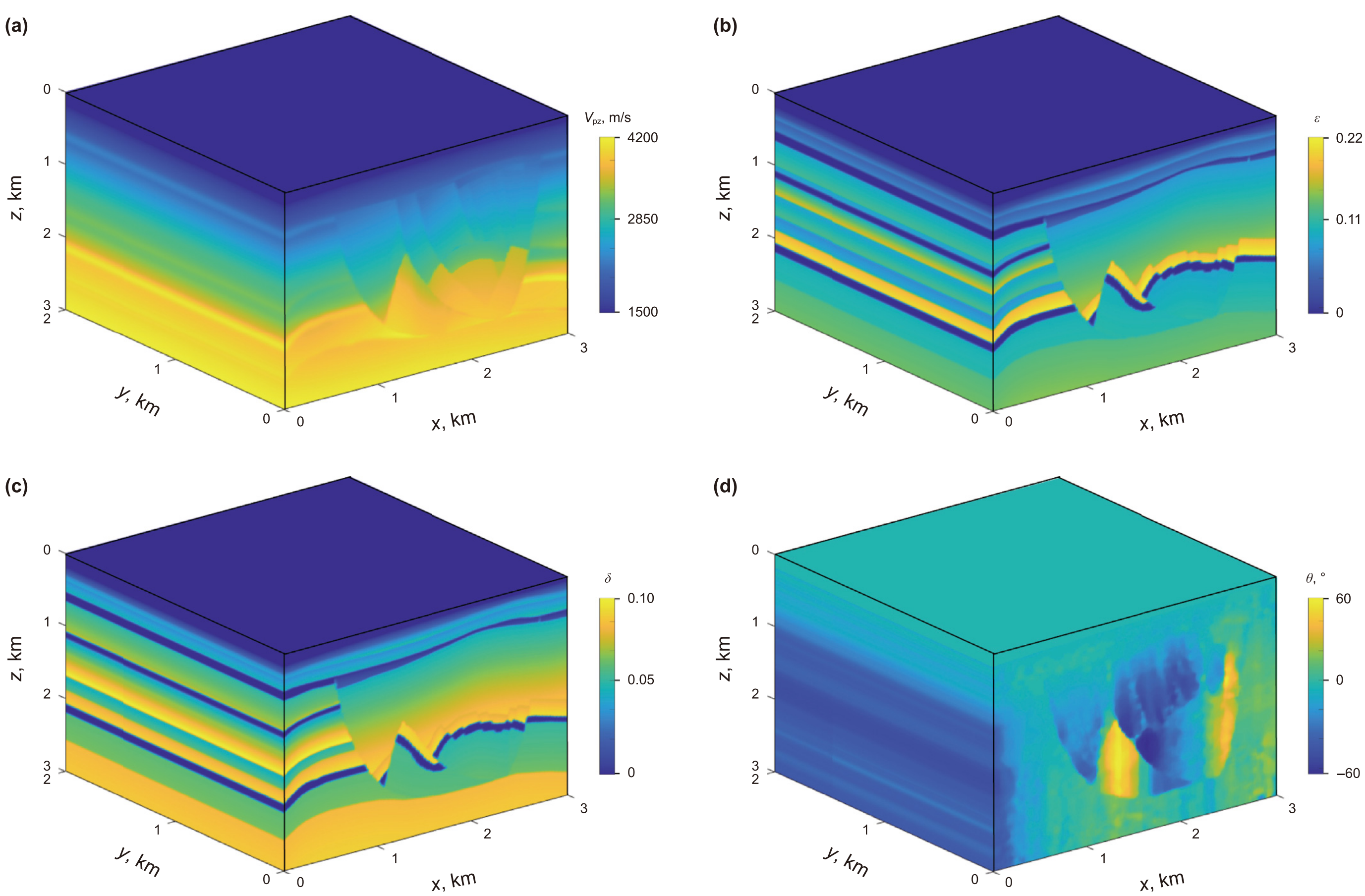

Fig. 7. The 3D modified BP 2007 TTI model. **(a)** V_{pz}, **(b)** ε, **(c)** δ, **(d)** θ.

models for TOA media, we adopt part of the 3D modified BP 2007 TTI model to implement the anisotropic wavefield simulation, which further reveals the accuracy and stability advantages of our approaches. Fig. 7 shows the 3D modified BP 2007 TTI model, including propagation velocity V_{pz}, Thomsen's anisotropic parameters ε and δ, and dip angle parameter θ, which are all established based on the standard 2D BP 2007 TTI model. The azimuth angle is constant $\phi = 30^\circ$. The model size is $(x, y, z) = (3000$ m, 2000 m,

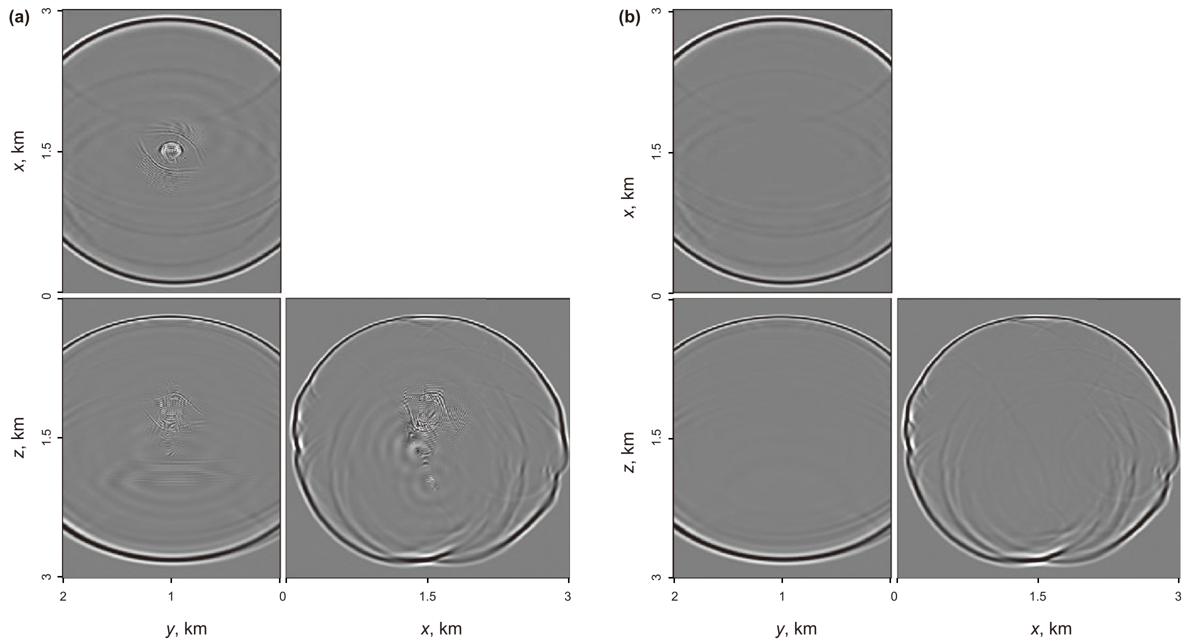

Fig. 8. Wavefield snapshots in 3D modified BP 2007 TTI model computed by **(a)** the conventional PWE and **(b)** the proposed PPE.

3000 m), and the cubic grid spacing is 10 m in all directions. We choose a 35 Hz Ricker wavelet at (1500 m, 1000 m, 1200 m) to generate the vibrations. Besides, the 3D hybrid absorbing boundary condition with 10 grid points are adopted to suppress unwanted artificial false reflections from truncated model boundaries (Liu and Sen, 2011). Fig. 8(a) depicts the time snapshot of wave propagation calculated by the traditional PWE. We can observe strong SV-wave and converted wave artifacts around the source, which may result in numerical instability during the wavefield extrapolation. By comparison, the time snapshot of our FD-based optimized PPE in Fig. 8(b) can thoroughly remove the SV-wave contamination, and thus produce highly accurate and stable pure P-wave events. In conclusion, the simulated results in the 3D complicated anisotropic media verify that our proposed scheme can effectively describe the pure P-wave propagation characteristics.

6. Discussion

In this section, we mainly analyze the limitations and potential solutions for our proposed scheme.

Compared with the presently available PPEs, the proposed equations derived from the optimization strategy have higher approximation accuracy because they distribute the numerical errors evenly within the whole wavenumber/frequency ranges. In additional, the FD-based numerical solutions have higher efficiency and flexibility than the conventional spectral-based method or hybrid pseudospectral method + FD method. The proposed method may damage the amplitude or phase features slightly, but these errors are completely acceptable for common anisotropy parameters (Xu and Zhou, 2014; Liang et al., 2023; Bitencourt and Pestana, 2024). Moreover, better approximation results can be achieved by further smoothing the model parameters, and we believe that the application of higher-order or optimized FD operators would resolve this issue. The computational accuracy may benefit from establishing a relation $\boldsymbol{n} = \mathbf{C}\boldsymbol{k}/|\boldsymbol{k}|$ between the unit vector of the phase direction $\boldsymbol{n}$ and the wavenumber vector $\boldsymbol{k}$, the operator $\mathbf{C}$ can be determined by an optimization method.

As mentioned above, the optimized polynomial coefficients in our scheme depend on anisotropic parameters. For a complex anisotropic model, the extra time needs to compute the coefficients. In practice, as described in the aforementioned “3D complicated anisotropic media” section, the modified BP 2007 TTI model shown in Fig. 7 is a pseudo 3D case. Therefore, we only need to calculate polynomial coefficients in the *xoz* plane. Coefficients in the 3D computational domain can be generated by extending the *xoz* plane along the *y* direction. The extra computational time of polynomial coefficients is acceptable compared with 3D wavefield extrapolation. As a potential solution, these coefficients can be precomputed by dividing the model parameters into fixed intervals (Zhang et al., 2019). Once we obtain the coefficients, we can store them in a local file and utilize them repeatedly. Thus, the computational efficiency can be guaranteed to some extent. Inevitably, the computational efficiency and storage are limitations of our present work for a 3D large-scale anisotropic model, especially for 3D cases in production. To reduce the computational cost, apart from the above parameter gridding and coefficient reutilization, maybe we can calculate partial coefficients and generate others by incorporating sparse representation and interpolation. More importantly, greater efforts must be made to achieve a significant computational accuracy, efficiency and storage for 3D production in our following works.

7. Conclusions

We proposed two modified pure qP-wave equations (PPEs) and illustrate their specific implementation scheme for seismic wavefield simulation in 3D TTI and TOA media. A combination of rational polynomial approximation and numerical optimization strategy is adopted to evaluate the original anisotropic dispersion relation, which includes complicated pseudo-differential operators, and further build two optimized PPEs for 3D TTI and TOA media. By introducing a scalar operator, the proposed equations are efficiently solved by incorporating the unit vector method and FD approach in the time-space domain. Theoretical derivations show that the structures of new equations are concise and the implementation processes are straightforward. Phase velocity analyses show that our proposed equations can produce reliable approximated results. Numerical examples verify that the newly derived PPEs can generate accurate P-wave events, completely free from SV-wave artifacts and instabilities. Besides, the proposed FD-based wavefield extrapolation strategy can omit the need for spectral-based transformation and other extra computational burden of the traditional solutions, thus the computational efficiency is significantly improved. In general, the development of these PPEs can be considered as an effective tool for anisotropic inversion and imaging in complex geologic structures.

CRediT authorship contribution statement

Shi-Gang Xu: Writing – review & editing, Writing – original draft, Visualization, Validation, Resources, Methodology, Investigation, Formal analysis, Data curation, Conceptualization. **Xing-Guo Huang:** Writing – review & editing, Visualization, Validation, Supervision, Methodology, Formal analysis. **Li Han:** Writing – review & editing, Visualization, Validation, Supervision, Methodology, Formal analysis.

Declaration of competing interest

The authors declare that they have no known competing financial interests or personal relationships that could have appeared to influence the work reported in this paper.

Acknowledgements

This research is supported by the National Key R&D Program of China (2021YFA0716902), National Natural Science Foundation of China (NSFC) under contract number 42374149 and 42004119, National Science and Technology Major Project (2024ZD1002907).

Appendix A. A simplified 3D TTI pure qP-wave equation

Starting from the exact TTI pure qP-wave dispersion relation (Eq. (1)), Zhan et al. (2012) derived a decoupled 3D TTI PPE in the time-wavenumber domain based on the first-order TE method as follows:

$$\frac{1}{V_{pz}^2}\frac{\partial^2 P(\boldsymbol{k},t)}{\partial t^2} = -\left\{\begin{array}{l} a_{11}k_x^2+a_{22}k_y^2+a_{33}k_z^2+a_{12}k_xk_y+a_{13}k_xk_z+ \\ a_{23}k_yk_z+a_{1111}\frac{k_x^4}{k^2}+a_{2222}\frac{k_y^4}{k^2}+a_{3333}\frac{k_z^4}{k^2}+ \\ \frac{k_x^3}{k^2}(a_{1112}k_y+a_{1113}k_z)+\frac{k_y^3}{k^2}(a_{1222}k_x+a_{2223}k_z)+ \\ \frac{k_z^3}{k^2}(a_{1333}k_x+a_{2333}k_y)+\frac{k_x^2}{k^2}\left(a_{1122}k_y^2+a_{1133}k_z^2\right)+ \\ a_{2233}\frac{k_y^2k_z^2}{k^2}+\frac{k_xk_yk_z}{k^2}(a_{1123}k_x+a_{1223}k_y+a_{1233}k_z) \end{array}\right\}P(\boldsymbol{k},t) \tag{A1}$$

in which, the polynomial coefficients are consisted of anisotropic parameters (ε, δ) and angle parameters (θ, ϕ). They have the following analytical forms (Zhan et al., 2012):

$$\left\{\begin{array}{l} a_{11}=(1+2\varepsilon)+2(\delta-2\varepsilon)\sin^2\theta\cos^2\phi \\ a_{22}=(1+2\varepsilon)+2(\delta-2\varepsilon)\sin^2\theta\sin^2\phi \\ a_{33}=(1+2\varepsilon)+2(\delta-2\varepsilon)\cos^2\theta \\ a_{12}=2(\delta-2\varepsilon)\sin^2\theta\sin 2\phi \\ a_{13}=2(\delta-2\varepsilon)\sin 2\theta\cos\phi \\ a_{23}=2(\delta-2\varepsilon)\sin 2\theta\sin\phi \\ a_{1111}=2(\varepsilon-\delta)\sin^4\theta\cos^4\phi \\ a_{2222}=2(\varepsilon-\delta)\sin^4\theta\sin^4\phi \\ a_{3333}=2(\varepsilon-\delta)\cos^4\theta \\ a_{1112}=4(\varepsilon-\delta)\sin^4\theta\sin 2\phi\cos^2\phi \\ a_{1113}=4(\varepsilon-\delta)\sin 2\theta\sin^2\theta\cos^3\phi \\ a_{1222}=4(\varepsilon-\delta)\sin^4\theta\sin 2\phi\sin^2\phi \\ a_{2223}=4(\varepsilon-\delta)\sin 2\theta\sin^2\theta\sin^3\phi \\ a_{1333}=4(\varepsilon-\delta)\sin 2\theta\cos^2\theta\cos\phi \\ a_{2333}=4(\varepsilon-\delta)\sin 2\theta\cos^2\theta\sin\phi \\ a_{1122}=3(\varepsilon-\delta)\sin^4\theta\sin^2 2\phi \\ a_{1133}=3(\varepsilon-\delta)\sin^2 2\theta\cos^2\phi \\ a_{2233}=3(\varepsilon-\delta)\sin^2 2\theta\sin^2\phi \\ a_{1123}=6(\varepsilon-\delta)\sin 2\theta\sin^2\theta\sin 2\phi\cos\phi \\ a_{1223}=6(\varepsilon-\delta)\sin 2\theta\sin^2\theta\sin 2\phi\sin\phi \\ a_{1233}=3(\varepsilon-\delta)\sin^2 2\theta\sin 2\phi \end{array}\right. \tag{A2}$$

Knowing that (Bitencourt and Pestana, 2024)

$$\left\{\begin{array}{l} \frac{k_x^2k_z^2}{k^2}=\frac{1}{2}\left(k_x^2-k_y^2+k_z^2-\frac{k_x^4}{k^2}+\frac{k_y^4}{k^2}-\frac{k_z^4}{k^2}\right) \\ \frac{k_x^2k_y^2}{k^2}=\frac{1}{2}\left(k_x^2+k_y^2-k_z^2-\frac{k_x^4}{k^2}-\frac{k_y^4}{k^2}+\frac{k_z^4}{k^2}\right) \\ \frac{k_y^2k_z^2}{k^2}=\frac{1}{2}\left(-k_x^2+k_y^2+k_z^2+\frac{k_x^4}{k^2}-\frac{k_y^4}{k^2}-\frac{k_z^4}{k^2}\right) \\ \frac{k_xk_yk_z^2}{k^2}=k_xk_y-\frac{k_x^3k_y}{k^2}-\frac{k_xk_y^3}{k^2} \\ \frac{k_x^2k_yk_z}{k^2}=k_yk_z-\frac{k_y^3k_z}{k^2}-\frac{k_yk_z^3}{k^2} \\ \frac{k_xk_y^2k_z}{k^2}=k_xk_z-\frac{k_x^3k_z}{k^2}-\frac{k_xk_z^3}{k^2} \end{array}\right. \tag{A3}$$

Using the above relationship, Eq. (A1) can be further simplified as (Bitencourt and Pestana, 2024)

$$\frac{1}{V_{pz}^2}\frac{\partial^2 P(\boldsymbol{k},t)}{\partial t^2} = -\left\{\begin{array}{l} \tilde{a}_{11}k_x^2+\tilde{a}_{22}k_y^2+\tilde{a}_{33}k_z^2+\tilde{a}_{12}k_xk_y+\tilde{a}_{13}k_xk_z+\tilde{a}_{23}k_yk_z \\ +\tilde{a}_{1111}\frac{k_x^4}{k^2}+\tilde{a}_{2222}\frac{k_y^4}{k^2}+\tilde{a}_{3333}\frac{k_z^4}{k^2}+ \\ \frac{k_x^3}{k^2}(\tilde{a}_{1112}k_y+\tilde{a}_{1113}k_z)+\frac{k_y^3}{k^2}(\tilde{a}_{1222}k_x+\tilde{a}_{2223}k_z)+ \\ \frac{k_z^3}{k^2}(\tilde{a}_{1333}k_x+\tilde{a}_{2333}k_y) \end{array}\right\}P(\boldsymbol{k},t) \tag{A4}$$

in which

$$
\begin{cases}
\tilde{a}_{11} = a_{11} + a_{1133}/2 + a_{1122}/2 - a_{2233}/2 \\
\tilde{a}_{22} = a_{22} - a_{1133}/2 + a_{1122}/2 + a_{2233}/2 \\
\tilde{a}_{33} = a_{33} + a_{1133}/2 - a_{1122}/2 + a_{2233}/2 \\
\tilde{a}_{12} = a_{12} + a_{1233}, \tilde{a}_{13} = a_{13} + a_{1223}, \tilde{a}_{23} = a_{23} + a_{1123} \\
\tilde{a}_{1111} = a_{1111} - a_{1133}/2 - a_{1122}/2 + a_{2233}/2 \\
\tilde{a}_{2222} = a_{2222} + a_{1133}/2 - a_{1122}/2 - a_{2233}/2 \\
\tilde{a}_{3333} = a_{3333} - a_{1133}/2 + a_{1122}/2 - a_{2233}/2 \\
\tilde{a}_{1112} = a_{1112} - a_{1233}, \tilde{a}_{1113} = a_{1113} - a_{1223} \\
\tilde{a}_{1222} = a_{1222} - a_{1233}, \tilde{a}_{2223} = a_{2223} - a_{1123} \\
\tilde{a}_{1333} = a_{1333} - a_{1223}, \tilde{a}_{2333} = a_{2333} - a_{1123}
\end{cases}
\tag{A5}
$$

Appendix B. Reference solutions based on the pseudospectral method for 3D TTI and TOA media

For exact pure qP-wave dispersion relation (Eq. (1)) in 3D TTI media, we can adopt the pseudospectral method to solve it and generate the reference solution. The corresponding time-wavenumber domain TTI pure qP-wave equation therefore is

$$
\frac{\partial^2 P(\boldsymbol{k},t)}{\partial t^2} = \frac{V_{pz}^2}{2}\left\{ \begin{array}{l} (1+2\varepsilon)\left[F^{-1}(-\widehat{k}_x\overline{P}) + F^{-1}(-\widehat{k}_y\overline{P})\right] + \\ F^{-1}(-\widehat{k}_z\overline{P}) + F^{-1}\left[-\beta(\widehat{k}_x,\widehat{k}_y,\widehat{k}_z)\overline{P}\right] \end{array} \right\}
\tag{B1}
$$

where, $\overline{P}$ is the spatial Fourier transform of P, F^{-1} denotes the inverse spatial Fourier transform, and $\beta(\widehat{k}_x, \widehat{k}_y, \widehat{k}_z) = \sqrt{f^2(\widehat{k}_x,\widehat{k}_y,\widehat{k}_z) - 8(\varepsilon-\delta)(\widehat{k}_x^2 + \widehat{k}_y^2)\widehat{k}_z^2}$.

Similarly, we apply the pseudospectral method to calculate the exact TOA dispersion relation (18) and produce the reference solution as follows:

$$
\frac{\partial^2 P(\boldsymbol{k},t)}{\partial t^2} = \frac{V_{pz}^2}{3}\left\{ -F^{-1}\left[-\kappa(\widehat{k}_x,\widehat{k}_y,\widehat{k}_z)\overline{P}\right]\right\}
\tag{B2}
$$

where $\kappa(\widehat{k}_x,\widehat{k}_y,\widehat{k}_z) = \left(-a - \sqrt[3]{(d+g)/2} - \sqrt[3]{(d-g)/2}\right)$

The derivations of Eqs. (B1) and (B2) are based on exact dispersion relations, therefore they can be considered as reference solutions for homogeneous anisotropic media (Chu et al., 2011; Zhan et al., 2012). For heterogeneous media, directly adopting the pseudospectral method to compute exact anisotropic dispersion relations may lead to numerical error and instability, thus many approximated schemes get further developments.

References

Alkhalifah, T., 2000. An acoustic wave equation for anisotropic media. Geophysics 65 (4), 1239–1250. https://doi.org/10.1190/1.1444815.

Alkhalifah, T., 2003. An acoustic wave equation for orthorhombic anisotropy. Geophysics 68 (4), 1169–1172. https://doi.org/10.1190/1.1598109.

Bitencourt, L.S., Pestana, R.C., 2024. Simplified TTI pure qP-wave equation implemented in the space domain and applied for reverse time migration in TTI media. Geophysics 89 (1), C17–C28. https://doi.org/10.1190/geo2022-0686.1.

Chu, C., Macy, B.K., Anno, P.D., 2011. Approximation of pure acoustic seismic wave propagation in TTI media. Geophysics 76 (5), WB97–WB107. https://doi.org/10.1190/geo2011-0092.1.

Du, X., Bancroft, J.C., Lines, L.R., 2007. Anisotropic reverse-time migration for tilted TI media. Geophys. Prospect. 55 (6), 853–869. https://doi.org/10.1111/j.1365-2478.2007.00652.x.

Duveneck, E., Bakker, P.M., 2011. Stable P-wave modeling for reverse time migration in tilted TI media. Geophysics 76 (2), S65–S75. https://doi.org/10.1190/1.3533964.

Fletcher, R.P., Du, X., Fowler, P.J., 2009. Reverse time migration in tilted transversely isotropic (TTI) media. Geophysics 74 (6), WCA179–WCA187. https://doi.org/10.1190/1.3269902.

Fomel, S., Ying, L., Song, X., 2013. Seismic wave extrapolation using lowrank symbol approximation. Geophys. Prospect. 61, 526–536. https://doi.org/10.1111/j.1365-2478.2012.01064.x.

Fowler, P.J., Du, X., Fletcher, R.P., 2010. Coupled equations for reverse time migration in transversely isotropic media. Geophysics 75 (1), S11–S22. https://doi.org/10.1190/1.3294572.

Guitton, A., Alkhalifah, T., 2017. A parameterization study for elastic VTI full waveform inversion of hydrophone components: synthetic and North Sea field data examples. Geophysics 82 (6), R299–R308. https://doi.org/10.1190/geo2017-0073.1.

Kazei, V., Alkhalifah, T., 2018. Waveform inversion for orthorhombic anisotropy with P-waves: feasibility and resolution. Geophys. J. Int. 213 (2), 963–982. https://doi.org/10.1093/gji/ggy034.

Li, B.W., Stovas, A., 2021. Decoupled approximation and separate extrapolation of P and SV-waves in transversely isotropic media. Geophysics 86 (4), C133–C142. https://doi.org/10.1190/geo2020-0232.1.

Li, X.Y., Zhu, H.J., 2018. A finite-difference approach for solving pure quasi-P-wave equations in transversely isotropic and orthorhombic media. Geophysics 83 (4), C161–C172. https://doi.org/10.1190/geo2017-0405.1.

Liang, K., Cao, D.P., Sun, S.R., Yin, X.Y., 2023. Decoupled wave equation and forward modeling of qP wave in VTI media with the new acoustic approximation. Geophysics 88 (1), WA335–WA344. https://doi.org/10.1190/geo2022-0292.1.

Liu, F., Morton, S.A., Jiang, S., Ni, L., Leveille, J.P., 2009. Decoupled wave equations for P and SV waves in an acoustic VTI media. 79th Ann. Int. Meet. SEG, Expand. Abstr. 2844–2848. https://doi.org/10.1190/1.3255440.

Liu, Y., 2013. Globally optimal finite-difference schemes based on least squares. Geophysics 78 (4), T113–T132. https://doi.org/10.1190/geo2012-0480.1.

Liu, Y., Sen, M.K., 2011. 3D acoustic wave modelling with time-space domain dispersion-relation-based finite-difference schemes and hybrid absorbing boundary conditions. Explor. Geophys. 42, 176–189. https://doi.org/10.1071/EG11007.

Mao, Q., Huang, J., Mu, X., 2024. Accurate simulations of pure-viscoacoustic wave propagation in tilted transversely isotropic media. Pet. Sci. 21 (2), 866–884. https://doi.org/10.1016/j.petsci.2023.11.005.

Masmoudi, N., Alkhalifah, T., 2018. Full waveform inversion in acoustic orthorhombic media and application to a North Sea data set. Geophysics 83 (5), C179–C193. https://doi.org/10.1190/geo2017-0738.1.

Mu, X.R., Huang, J.P., Yong, P., Huang, J.Q., Guo, X., Liu, D.J., Hu, Z.D., 2020. Modeling of pure qP-and qSV-waves in tilted transversely isotropic media with the optimal quadratic approximation. Geophysics 85 (2), C71–C89. https://doi.org/10.1190/geo2018-0460.1.

Ren, Z.M., Dai, X., Wang, L., 2024a. Full-waveform inversion of pure quasi-P waves in titled transversely isotropic media based on different parameterizations. Geophysics 89 (2), C57–C73. https://doi.org/10.1190/geo2023-0367.1.

Ren, Z.M., Wang, L., Bao, Q.Z., 2024b. Truncated Gauss-Newton full-waveform inversion of pure quasi-P waves in vertical transverse isotropic media. Pet. Sci. 21 (5), 3102–3124. https://doi.org/10.1016/j.petsci.2024.04.017.

Song, X., Alkhalifah, T., 2013. Modeling of pseudo-acoustic P-waves in orthorhombic media with a low-rank approximation. Geophysics 78 (4), C33–C40. https://doi.org/10.1190/geo2012-0144.1.

Sun, B., Alkhalifah, T., 2021. Pseudoelastic pure P-mode wave equation. Geophysics 86 (6), 57–V508. https://doi.org/10.1190/geo2021-0084.1.

Thomsen, L., 1986. Weak elastic anisotropy. Geophysics 51 (10), 1954–1966. https://doi.org/10.1190/1.1442051.

Tsvankin, I., 1997. Anisotropic parameters and P-wave velocity for orthorhombic media. Geophysics 62 (4), 1292–1309. https://doi.org/10.1190/1.1444231.

Tsvankin, I., Grechka, V., 2011. Seismology of azimuthally anisotropic media and seismic fracture characterization. Soc. Explor. Geophys. https://doi.org/10.1190/1.9781560802839.

Wang, Z., 2002. Seismic anisotropy in sedimentary rocks, part 2: laboratory data. Geophysics 67 (5), 1423–1440. https://doi.org/10.1190/1.1512743.

Waheed, U.B., Alkhalifah, T., Wang, H., 2015. Efficient traveltime solutions of the acoustic TI eikonal equation. J. Comput. Phys. 282, 62–76. https://doi.org/10.1016/j.jcp.2014.11.006.

Wu, Z., Alkhalifah, T., 2014. The optimized expansion based low-rank method for wavefield extrapolation. Geophysics 79 (2), T51–T60. https://doi.org/10.1190/geo2013-0174.1.

Xu, S., Zhou, H., 2014. Accurate simulations of pure quasi-P-waves in complex anisotropic media. Geophysics 79 (6), T341–T348. https://doi.org/10.1190/geo2014-0242.1.

Xu, S., Liu, Y., 2018. Effective modeling and reverse-time migration for novel pure acoustic wave in arbitrary orthorhombic anisotropic media. J. Appl. Geophys. 150, 126–143. https://doi.org/10.1016/j.jappgeo.2018.01.013.

Xu, S., Bao, Q., Ren, Z., 2023. Target-oriented Q-compensated reverse-time migration by using optimized pure-mode wave equation in anisotropic media. Pet. Sci. 20 (2), 866–878. https://doi.org/10.1016/j.petsci.2022.12.016.

Xu, S., Stovas, A., Alkhalifah, T., Mikada, H., 2020. New acoustic approximation for the transversely isotropic media with a vertical symmetry axis. Geophysics 85 (1), C1–C12. https://doi.org/10.1190/geo2019-0100.1.

Xu, S., Stovas, A., 2021. Perturbation-based travel time approximation for two acoustic assumptions in the transversely isotropic media with a vertical symmetry axis. Geophys. Prospect. 69, 1591–1605. https://doi.org/10.1111/1365-2478.13131.

Yan, J., Liu, H., 2016. Modeling of pure acoustic wave in tilted transversely isotropic media using optimized pseudo-differential operators. Geophysics 81 (3), T91–T106. https://doi.org/10.1190/geo2015-0111.1.

Zhan, G., Pestana, R.C., Stoffa, P.L., 2012. Decoupled equations for reverse time

migration in tilted transversely isotropic media. Geophysics 77 (2), T35–T45. https://doi.org/10.1190/geo2011-0175.1.
Zhang, H., Zhang, Y., 2008. Reverse time migration in 3D heterogeneous TTI media. 78th Ann. Int. Meet. SEG, Expand. Abstr. 2196–2200. https://doi.org/10.1190/1.3059322.
Zhang, H., Zhang, Y., 2011. Reverse time migration in vertical and tilted orthorhombic media. 81th Ann. Int. Meet. SEG, Expand. Abstr 185–189. https://doi.org/10.1190/1.3627568.
Zhang, H., Zhang, G., Zhang, Y., 2009. Removing S-wave noise in TTI reverse time migration. 79th Ann. Int. Meet. SEG, Expand. Abstr. 2849–2853. https://doi.org/10.1190/1.3255441.
Zhang, Y., Liu, Y., Xu, S., 2019. Efficient modelling of optimized pure acoustic wave equation in 3D transversely isotropic and orthorhombic anisotropic media. Explor. Geophys. 50 (5), 561–574. https://doi.org/10.1080/08123985.2019.1643680.
Zhang, Y., Zhang, H., Zhang, G., 2011. A stable TTI reverse time migration and its implementation. Geophysics 76 (3), WA3–WA11. https://doi.org/10.1190/1.3554411.